CD11B^{+}CD36^{+} cells are bone anabolic macrophages that limit age-associated bone loss

Short title: Age-associated cortical bone remodeling

Jinsha Koroth[1], Ismael Y. Karkache[1,2], Elizabeth K. Vu[1], Kim C. Mansky[2,3] and Elizabeth W. Bradley[1,4*]

1-Department of Orthopedic Surgery, University of Minnesota, Minnesota, United States of America

2-College of Veterinary Sciences, University of Minnesota, Minnesota, United States of America

3-School of Dentistry, University of Minnesota, Minnesota, United States of America

4-Stem Cell Institute, University of Minnesota, Minnesota, United States of America

*Corresponding author

E-mail address: ebradle1@umn.edu

Key words: bone, osteoclast, osteomac, bone remodeling, osteoclast progenitor, osteoprogenitor, osteoblast

ABSTRACT

Disruptions in the bone remodeling cycle that occur with increasing age lead to degeneration of the skeleton and increased risk of fragility fractures. Our understanding of how bone remodeling within cortical bone is controlled and altered with age in males and females is limited. Here, we generated bone marrow chimeric mice to understand the impacts of age and sex on bone remodeling. We demonstrate that transplantation of aged male or female bone marrow into young, lethally irradiated male hosts unexpectedly enhances cortical bone mass without impacting cancellous bone. Our single cell RNA-sequencing data show that mice reconstituted with aged bone marrow exhibited subsets of cells marked by CD11B/CD36 expression that demonstrate enhanced production of anabolic cytokines as compared to young counterparts, and that these myeloid subsets exist under conditions of normal physiology in aged mice. Importantly, $CD11B^{+}CD36^{+}$ cells do not differentiate into osteoclasts in vitro, and CD36 does not mark TRAP+ cells in vivo. Instead, $CD36^{+}$ cells localize to resorption sites, including within cortical bone defects, suggesting their involvement in cortical bone remodeling and healing. $CD11B^{+}CD36^{+}$ cells also express elevated levels of bone anabolic WNT ligands, especially Wnt6. In functional assays, we demonstrate that soluble factors produced by $CD11B^{+}CD36^{+}$ cells enhance osteoblast progenitor commitment, mineralization, and activation of WNT signaling in vitro. Moreover, CD11B/CD36 exquisitely mark a subset of anabolic myeloid cells within human bone marrow. In conclusion, our studies identified a novel population of aged macrophages that limit cortical bone loss.

INTRODUCTION

Bone mass in men and women starts to decline during the third decade of life (1). Women also exhibit a punctuated period of bone loss following menopause proceeded by age-associated declines in bone mass at a rate approaching that of men (2). In both men and women, age constitutes the greatest risk for a fragility fracture (3). Half of all women and one quarter of men are projected to suffer an age-related low bone mass fracture (4). Importantly, approximately 25% of individuals die a year after a hip fracture (5-9);

49 thus, a better understanding of the pathophysiology of age-related declines in bone mass would aid in the
50 development of preventative and interventional strategies.

51 Cortical bone comprises the majority of skeletal bone mass (80%), and accounts for 70% of bone lost with
52 age (10, 11). Although bone anabolic agents enhance vertebral cortical bone mass, efficacy is lower at the
53 hip (+3.9%) compared to the spine (+12.3%) (12, 13); therefore, additional therapeutics improving cortical
54 bone are desperately needed.

55 The process of bone remodeling facilitates homeostasis of the adult skeleton. Bone remodeling consists
56 of the activation, resorption, reversal, and formation phases (14). Aging disrupts these phases, resulting
57 in unbalanced bone formation and bone resorption (14). Osteoclasts mediate bone resorption, whereas
58 osteoblasts orchestrate formation. While the coupled cellular activities of osteoclasts and osteoblasts
59 maintain optimal bone health, recent evidence suggests that macrophages within the bone niche help
60 coordinate the bone remodeling process (14). In spite of this, we understand little about how different
61 subsets of macrophages impact the bone remodeling. In this study, we sought to define how age affects
62 macrophage types and examine the impact of those cells on cortical and trabecular bone homeostasis.

63 **RESULTS**

64 **Transplantation of aged bone marrow into young hosts promotes cortical bone mass**

65 Recent work supports that myeloid cells residing within the bone marrow regulate bone remodeling
66 during conditions of both normal physiology and pathological conditions (15, 16). Lower peak bone mass
67 and acute bone loss following the menopause predisposes women to osteoporosis and greater risk of
68 fracture with age; however, it is unclear if rapid bone loss associated with sex steroid deficiency and age-
69 associated bone loss are mediated by the same mechanisms, or if there are differences in how age-
70 associated bone loss occurs in males and females. To understand the cellular mechanisms driving bone
71 loss prior to reproductive senescence, we performed bone marrow transplantation assays generating

72 chimeric mice. We started with young (e.g., 6-week-old) male recipient mice (Figure 1A, left panel). Young
73 recipient male mice were lethally irradiated to ablate the bone marrow. In parallel, we collected bone
74 marrow from 6- or 40-week-old donor male or female mice (Figure 1A, right panel). Donor bone marrow
75 was depleted of T cells through magnetic-assisted cell sorting (MACS)-mediated removal of CD3+ and
76 CD8+ cells. Young recipient mice were then reconstituted with T-cell depleted donor bone marrow from
77 mice of one of four groups (Figure 1A, right panel) (17-19). We then aged recipient male mice to six-
78 months (e.g., 18-weeks after BM transplantation). To estimate percent chimerism, we collected bone
79 marrow and liver cells from male recipient mice transplanted with female bone marrow, and assessed
80 expression of X- and Y-linked genes. Within the bone marrow, male recipient mice showed robust
81 expression of X-linked genes *Xist* and *Gata1*, but little to no expression of Y-linked genes *Sry* and *Ddx3y*
82 (Figure 1B), supporting that cells within the bone marrow of ablated recipient males were reconstituted
83 by female cells. In contrast, X- and Y-linked genes were expressed within the male recipient liver. Gross
84 examination showed that male mice receiving bone marrow from either aged males (group 2) or aged
85 females (group 4) exhibited signs of premature aging (e.g., gray coat color) (Figure 1C). Body weight was
86 also reduced by transplantation of aged male bone marrow (e.g., group 2), but no other significant weight
87 changes were observed (Figure 1D). Splenomegaly can point to deficiencies in bone marrow function, so
88 we also assessed the spleen weight to body weight ratio. Changes in body weight-adjusted spleen mass
89 were not observed within any group (Figure 1E).

90 We next assessed bone mass of 24-week-old recipient male mice. We first determined how irradiation
91 affected cortical bone by comparing chimeric mice within each group to 24-week-old non-irradiated
92 controls. We noted that irradiation decreased cortical BV/TV (Figure 2A, D), but did not alter cortical
93 thickness (Figure 2B, D) or trabecular BV/TV (Figure 2D, E) when comparing non-irradiated controls to
94 male mice transplanted with sex- and age-matched bone marrow (e.g., group 1 vs NI). Likewise, enodsteal

95 perimeter was significantly increased when comparing to non-irradiated controls (Figure 2C). In contrast,
96 irradiation increased trabecular spacing but reduced trabecular thickness (Figure 2D, F, G).

97 We next assessed changes between groups 1 and 2 to determine the effect that aged, but sex-matched
98 bone marrow had on cortical and trabecular bone. Micro-CT analyses of the resulting chimeric mice in
99 groups 1 and 2 revealed a surprising increase cortical bone mass (+10%) and cortical thickness (+7%) when
100 male recipients were reconstituted with sex-matched, but aged bone marrow (Figure 2A, B, D). In
101 contrast, no changes in trabecular BV/TV were observed between these groups (Figure 2D, E), but we did
102 note increased trabecular spacing coupled with diminished trabecular thickness (Figure 2D, F, G). These
103 data suggested that transplantation of aged bone marrow enhanced cortical but not trabecular bone
104 mass.

105 We next examined the effects transplantation of bone marrow derived from female mice on bone mass.
106 When comparing young male mice reconstituted with bone marrow from age-matched males or females
107 (groups 1 and 3), we did not see a change in cortical BV/TV or cortical thickness (Figure 2A, B, D). Likewise,
108 trabecular BV/TV, trabecular number, and trabecular spacing were unchanged (Figure 2D-F), but we did
109 observe a slight reduction in trabecular thickness when comparing these groups (Figure 2G).

110 We next compared young male mice transplanted with either sex- and age-matched bone marrow to
111 those transplanted with bone marrow collected from 40-week-old females (groups 1 and 4). We noted
112 increased cortical BV/TV, but no significant changes in cortical thickness (Figure 2A, B, D). No changes in
113 trabecular bone parameters were noted (Figure 2D-G). We then compared the effects of age when
114 transplanting female bone marrow (e.g., groups 3 versus 4). Reconstitution of young male mice with aged
115 female bone marrow enhanced cortical BV/TV as compared to age-matched female bone marrow, but did
116 not alter cortical thickness (Figure 2A, B, D). No changes in trabecular BV/TV, trabecular number, or
117 trabecular spacing were noted (Figure 2D-F), but we did observe an increase in trabecular thickness

118 (Figure 2G). These results mirror those we observed when aged male bone marrow was transplanted into
119 young male recipients.

120 Enhanced cortical bone mass could be due to increased bone formation and/or a reduction in bone
121 resorption at the periosteal or endosteal surfaces, respectively. To determine how bone remodeling was
122 altered within our chimeric mice we examined periosteal and endosteal cortical bone perimeter.
123 Irradiation increased endosteal perimeter when comparing mice within group 1 to non-irradiated
124 controls, supporting that irradiation increases resorption at the endosteal surface. In contrast, mice
125 transplanted with aged bone marrow within group 2 exhibited decreased endosteal perimeter (Figure 2C).
126 Likewise, transplantation of female bone marrow diminished endosteal perimeter (Figure 2C). These
127 results suggest that transplantation of aged bone marrow reduced endosteal resorption of cortical bone
128 or lead to increased endosteal formation.

129 **Subsets of myeloid cells from aged bone marrow associate with enhanced cortical bone**

130 Our results from the bone marrow transplantation assays combined with recent work demonstrating that
131 myeloid lineage cells (e.g., erythromyeloid progenitors, osteoclasts, osteomorphs, osteomacs) regulate
132 the bone remodeling process, suggest the existence of aged myeloid cells that promote maintenance of
133 cortical, but not trabecular bone. Moreover, a recent study demonstrated that erythromyeloid
134 progenitors expand during intensive hematopoietic regeneration (20); therefore, we profiled myeloid
135 cells within the bone marrow of our chimeric mice. We first evaluated the cellular subsets in young male
136 recipients transplanted with sex-matched bone marrow derived from either age-matched or 40-week-old
137 mice via singe cell RNA-sequencing (scRNA-Seq) of $CD11B^+$ cells. Integration of these two datasets did not
138 uncover unique clusters (Figure 3A), but we noted differential gene expression within clusters when
139 comparing $CD11B^+$ cells from mice reconstituted with aged as compared to age-matched bone marrow
140 from either males (Figure 3) or females (Figure 4).

141 In mice reconstituted with male cells, all clusters expressed markers for hematopoietic cells, including
142 *Cd45*, *Pu.1* and *Chi3l* (Figure 3B-D). We also noted multiple *Csf1r*$^+$ clusters, including clusters 1, 4, 7, 8, 14,
143 15, and 16 (Figure 3E, R). Expression of *Kit* and *Myb* marked highly proliferative cells within clusters 6 and
144 12, which are likely myeloid progenitor cells (Figure 3F, G). Macrophage markers *F4/80*, *Cd68*, and *Cd86*
145 were likewise expressed by cells within clusters 1, 4, 7, 8, and 14-16 (Figure 3H-J). The putative osteomac
146 marker *Cd166* (21) was broadly expressed (Figure 3K), whereas the macrophage marker *Mrc1* was mostly
147 restricted to clusters 14-16 (Figure 3L, R). Cells within cluster 16 expressed the highest levels of *Mrc1*, but
148 expression was diminished by cells within cluster 15 (Figure 3L, R). Similarly, expression of *Cx3cr1* was
149 restricted to clusters 14-16, with the highest expression observed by cells within cluster 15 (Figure 3M,
150 R). Some cells within cluster 14-16 also expressed *RANK* (Figure 3N), supporting the potential of these
151 cells to give rise to osteoclasts. We also noted high enrichment of *Cd74*, a putative osteomorph marker
152 (22), *Siglec1/Cd169*, and *Cd36* within clusters 14-16 (Figure 3O-R). Recent genetic evidence suggests that
153 cortical bone may be controlled specifically by several signaling pathways/components (e.g., Wnt and
154 Notch signaling) (23). We next evaluated expression of these and related genes across all clusters and
155 noted high expression of Bmps, Collagens, and Wnts by cells within clusters 14-16, and to some extent
156 cluster 17 (Figure 2R). Enrichment of B Cell markers distinguished cluster 17.

157 We next evaluated the effect of sex on subsets of CD11B$^+$ cells following intensive bone marrow
158 reconstitution. We integrated scRNA-Seq results from the CD11B$^+$ cells within the bone marrow of young
159 male mice reconstituted with either age-matched male bone marrow or 40-week-old female bone
160 marrow. This analysis did not reveal unique clusters (Figure 4A). As above, *Cd45*, *Pu.1*, and *Chi3l* were
161 broadly distributed (Figure 4B-D). *Csf1r*$^+$ clusters included clusters 1- 3, 11, 12, 15 and 17 (Figure 4E).
162 Myeloid progenitor cells marked by expression of *Kit* and *Myb* were contained within clusters 6 and 9
163 (Figure 4F, G). The cells within clusters 1-3, 5, 11, 12, 15, and 17 expressed the macrophage markers *F4/80*,
164 *Cd68*, and *Cd86* (Figure 4H-J); *Cd166* was broadly expressed (Figure 4K). In contrast, *Mrc1* was expressed

165 by cells within clusters 12 and 17 (Figure 4J, R). High expression of *Cx3cr1* marked cells within clusters 11
166 and 15, whereas expression was diminished with clusters 12 and 17 (Figure 4M, R). Expression of RANK
167 was observed by cells within clusters 11 and 15-17 (Figure 4N). High expression of *Cd74* was also noted
168 of clusters 11, 12 and 15-17 (Figure 4O, R), whereas *Cd36* was localized to cells within clusters 11, 12, 15
169 and 17, with cluster 11 exhibiting lower expression (Figure 4Q, R). As above, we noted enriched
170 expression of Bmps, Collagens, and Wnts by cells within clusters 12, 15 and 17 (Figure 4R). We observed
171 similar findings when comparing CD11B$^+$ cells from young male mice reconstituted with bone marrow
172 from 40-week-old males to those reconstituted with 40-week-old females, demonstrating that age, but
173 not sex of donor cells associated with enhanced cortical bone mass. Likewise, our data suggest that
174 specific subsets of CD11B$^+$ cells express bone anabolic genes, and that these subsets are delineated by
175 differential expression of *Cd36*.

176 **Characterization of CD11B$^+$ cellular subsets within the bone marrow of young and aged animals**

177 We noted the presence of several cellular subsets of cells within aged mice that expressed bone anabolic
178 genes. To broadly define the types of myeloid cells within the bone marrow and evaluate how age alters
179 these cellular subsets, we performed single cell RNA-sequencing (scRNA-Seq) on CD11B$^+$ cells from the
180 bone marrow of 8- or 40-week-old male and female C57Bl6/J mice. We chose these ages to reflect a period
181 of bone anabolism (e.g., gain in bone mass) during youth and a period of age-associated bone loss prior
182 to reproductive senescence. scRNA-Seq of CD11B$^+$ cells from young animals revealed multiple cells types,
183 including *RANK*$^+$ osteoclast progenitors, dendritic cells, neutrophils, monocytes, macrophages as well as
184 proliferative *Kit*$^+$/*Myb*$^+$ myeloid progenitors (Figure 5A, C).

185 We first examined macrophage clusters within young males and females. We noted two macrophage
186 clusters within 8-week-old CD11B-expressing bone marrow cells. Cluster 8 exhibited reduced expression
187 of *Csf1r*, *Cx3cr1* and *Cd74*, but higher expression of *Mrc1* and *Cd36* (Figure 5B). Cluster 8 showed
188 enrichment in bone anabolic genes such as BMPs, Collagens and Wnts. These bone anabolic proteins

189 were also expressed by *Csf1r*$^{-}$ cells within cluster 11. Likewise, we identified three *Csf1r*-expressing
190 clusters within CD11B^{+} cells derived from the bone marrow of 8-week-old females (Clusters 3, 4, and 6,
191 Figure 5C, D). Clusters 3 and 6 demonstrated reduced expression of *Csf1r*, but levels of *Mrc1* and *Cd36*
192 were greater (Figure 5D). Cluster 4 demonstrated the highest enrichment for *Csf1r* and *Cx3cr1*, but
193 exhibited little expression of *Cd36* or *Cd74*. Bone anabolic genes were enriched in clusters 3 and 6 (Figure
194 5D). These data pointed to a set of macrophages within the bone marrow that produce bone anabolic
195 factors.

196 When examining aged CD11B^{+} cells, we likewise noted several myeloid subsets that were analogous to
197 those present within young animals. Within males, we noted three subsets (clusters 4, 9, and 10) that all
198 showed enrichment for *Csf1r* and *Cx3cr1* (Figure 5E, F). Moreover, clusters 9 and 10 demonstrated high
199 expression of *Cd36*, but enrichment in *Cd74* by cells within cluster 9 and *Mrc1* by cells in cluster 10
200 differentiated these clusters (Figure 5F). All three clusters exhibited enrichment in Wnt gene expression,
201 but only clusters 9 and 10 significantly expressed Bmps. Within CD11B^{+} female ages cells, clusters 7, 8, 9,
202 and 14 all showed enrichment for *Csf1r*, *Mrc1* and *Cd36* (Figure 5G, H). *Cx3cr1* expression defined cluster
203 7 as well as cluster 9, but to a much lesser extent. *Cd74* also demonstrated differential expression
204 amongst these four clusters (Figure 5H). Cluster 7 showed limited expression of Bmps and Wnts, whereas
205 these bone anabolic genes were enriched amongst clusters 8, 9, and 14 (Figure 5H). These data highlight
206 subsets of CD11B^{+}/*Csf1r*$^{+}$ cells within the bone marrow of aged animals that can be delineated by
207 differential expression of *Cd74*, *Cx3cr1*, *Mrc1*, and/or *Cd36*.

208 **CD36+ cells associate with sites of bone resorption on endocortical surfaces**

209 *Cd36* represented one of the most highly differentially expressed genes in our scRNA-Seq analyses and
210 was exclusively expressed by specific subsets of cells within our analyses. We postulated that
211 CD11B^{+}CD36^{+} cells either serve as osteoclast progenitors or play a regulatory role in the bone remodeling

212 process given that they are enriched in chimeric mice with elevated cortical bone mass. To investigate
213 their localization and potential function, we performed immunohistochemical (IHC) staining for CD36 on
214 femur sections from 12- and 24-week-old female mice. We also examined sections of cortical bone defects
215 collected 14 days post-injury (24). To visualize bone remodeling sites, we additionally performed TRAP
216 staining. Our results showed that CD36 was diffusely expressed by cells within the BM cavity, with no
217 enrichment near cortical bone remodeling sites in 12-week-old female mice (Figure 6A, left column).
218 However, in 24-week-old mice and within cortical bone defects, we observed strong CD36 staining in cells
219 located near osteoclasts (Figure 6A, middle and right columns). CD36 expression by mature osteoclasts
220 was not detected under any conditions. These results suggest that $CD36^{HI+}$ cells may regulate bone
221 remodeling and regeneration.

222 To assess whether $CD11B^{+}CD36^{+}$ cells function as osteoclast progenitors, we isolated $CD11B^{+}CD36^{+}$ and
223 $CD11B^{+}CD36^{-}$ cells from the BM of 6-9-week-old female mice and cultured them under osteoclastogenic
224 conditions. While the $CD11B^{+}CD36^{-}$ population formed $TRAP^{+}$ multinucleated cells, indicative of
225 osteoclasts, the $CD11B^{+}CD36^{+}$ cultures only produced mononuclear cells (Figure 6B, lower panel). These
226 findings suggest that $CD11B^{+}CD36^{+}$ cells are involved in cortical bone regeneration and remodeling but do
227 not form osteoclasts, supporting previous reports (25).

228 **$CD11B^{+}CD36^{+}$ myeloid cells support bone formation**

229 Our scRNA-Seq analysis revealed that $CD11B^{+}CD36^{+}$ cells express several bone anabolic factors, including
230 *Wnt10b*, *Wnt6*, *Wnt3a*, *Bmp1*, and *Bmp2* (Figure 3R). To validate these findings, we FACS-sorted
231 $CD11B^{+}CD36^{+}$ cells from the bone marrow of 6-9-week-old female mice. $CD11B^{+}CD36^{+}$ cells comprised
232 8.7% of the isolated bone marrow cells (Figure 7A). We observed increased expression of *Wnt10b*, *Wnt6*,
233 and *Bmp1*, and reduced expression of *Wnt3a* and *Bmp2* by $CD11B^{+}CD36^{+}$ cells compared to $CD11B^{+}CD36^{-}$

234 cells (Figure 7B-F). *Wnt6* showed the most significant differential expression, which we further confirmed
235 by western blotting (Figure 7G).
236
237 Next, we investigated whether factors secreted by CD11B$^+$CD36$^+$ cells influence osteoprogenitor
238 proliferation, migration, commitment, and mineralization. CD11B$^+$CD36$^-$ and CD11B$^+$CD36$^+$ cells were
239 sorted from the BM of 6-9-week-old male and female C57Bl/J mice, cultured with M-CSF for three days,
240 and conditioned medium was collected. ST2 osteoprogenitor cells were then cultured in conditioned
241 medium for 24 hours to assess proliferation and migration (Figure 7H). Cck-8 assays indicated no
242 significant impact on osteoprogenitor proliferation and transwell assays similarly showed no significant
243 effects on migration. To evaluate osteoprogenitor commitment and mineralization, ST2 cells were
244 cultured in conditioned medium under osteogenic conditions. Enhanced mineralization was observed in
245 cultures treated with CD11B$^+$CD36$^+$ conditioned medium (Figure 7K, L) accompanied by increased
246 expression of *Bgn*, *Phospho1*, and *Sp7* (Figure 7M-O). Conversely, *Mmp13* and *Tnfrsf11*/RANKL expression
247 was reduced in these cultures (Figure 7P, Q). Finally, we assessed the activation of β-catenin and JNK
248 signaling pathways in ST2 cells cultured in conditioned medium from CD11B$^+$CD36$^-$ and CD11B$^+$CD36$^+$ cells
249 for one hour. Western blotting revealed elevated levels of active β-catenin and JNK phosphorylation,
250 indicating increased canonical and/or non-canonical Wnt signaling (Figure 7R). Likewise, NFAT1 and
251 TCF1/7 levels were enhanced (Figure 7R). These results suggest that CD11B$^+$CD36$^+$ cells produce WNT6,
252 which promotes osteoblast differentiation and bone formation.

253 **CD11B$^+$CD36$^+$ Cells within Human Bone Marrow**

254 To show that our results may translate to humans, we performed single cell sequencing of CD11B$^+$ cells
255 from the bone marrow aspirate of a 45-year-old human female. Using the pipeline described above, we
256 aligned data to the hg38 reference genome. We identified a cluster of isolated CD11B$^+$ cells exquisitely
257 defined by *Cd36* (Figure 8A, Q, R). CD11B$^+$CD36$^+$ cells within cluster 7 also expressed *Cd45*, *Pu.1*, *Csf1r*,

258 *F4/80*, *Cd68*, *Cd86*, *Cd166*, *Cd74*, and *Cx3cr1*, but were mostly negative for *Chi31l*, *Mrc1*, *RANK*, and
259 *Siglec1/Cd169* (Figure 8B-P). We also noted that expression of *Cd166*, the putative osteomac marker, and
260 *Cd74* were broadly expressed by CD11B$^+$ cells (Figure 8K, O). Expression of *Wnt6* was likewise restricted
261 to CD11B$^+$ cells cluster 7; thus, bone marrow from aged humans also contains an anabolic macrophage
262 population marked by CD11B/CD36.

263 **DISUCSSION**

264 The goal of our study was to examine how age and sex of hematopoietic cells affect skeletal aging. Prior
265 work documented that altered mesenchymal cell function facilitates age-associated changes to trabecular
266 bone, with consequent myeloid cell skewing (26, 27). Our study supports this finding, as we did not
267 observe changes to trabecular bone mass or microarchitecture. In contrast, our data support that age
268 alters bone marrow composition following intensive hematopoietic regeneration as previously described
269 (20), and those alterations in bone marrow composition facilitate gains in cortical bone. Moreover, our
270 data suggest that a subpopulation of aged macrophages limit endocortical bone resorption.

271 Bone resorbing osteoclasts can arise from hematopoietic stem cells or from long-lived erythro-myeloid
272 progenitors within the bone marrow. Osteoclasts have an estimated 6-month half-life in mice (28-30).
273 Recent evidence suggests that osteoclasts derived from different subsets of progenitors may facilitate
274 bone remodeling in different contexts (31-33). For instance, osteoclast progenitors that contribute to
275 homeostatic bone remodeling differ from those mediating bone loss associated with inflammatory
276 conditions (32). Osteoclasts that remodel bone in other perturbed states or within different bone
277 compartments may likewise differ. Our data suggest that age-associated resorption at endosteal cortical
278 bone surfaces may be distinct and limited by secreted factors produced CD11B$^+$CD36$^+$ cells. To the best of
279 our knowledge, this represents the first example of an aged myeloid cell type that limits bone resorption.

280 In our study, we identified a specific myeloid subset of aged cells that limit age-associated cortical bone
281 loss. Surface marker expression of CD11B and CD36 characterizes this subset of cells. In addition to these
282 surface markers, osteomorph markers (e.g., Axl, Cadm1, Ccr3, Cd74, Vcam1 (22)) were significantly
283 enriched within our identified myeloid subset. Osteomorphs have been speculated to function during the
284 reversal phase of bone remodeling. Given their proximity to bone resorbing osteoclasts along the cortical
285 surface, our identified cellular subset could be osteomorphs. Indeed, our scRNA-Seq analyses
286 demonstrated expression of RANK within these clusters, but we were unable to generate osteoclasts from
287 sorted $CD11B^{+}CD36^{+}$ cells in vitro. In contrast, $CD11B^{+}CD36^{-}$ cells efficiently formed osteoclasts in vitro.
288 These data suggest that our identified myeloid subset is potentially distinct from osteomorphs, but we do
289 not know if $CD11B^{+}CD36^{+}$ cells could fuse with existing osteoclasts in vivo.

290 CD36 is a cell surface marker delineating our population of interest, but we are unsure if CD36 is merely
291 a marker for this myeloid subset, or if CD36 plays a functional role in controlling age-associated cortical
292 bone loss. CD36 is a membrane glycoprotein that functions as a scavenger receptor for various ligands,
293 including collagen, thrombospondin-1, anionic phospholipids, and long chain fatty acids. While CD36 is
294 broadly expressed, adipocytes, cardiac myocytes, and immune cells including myeloid cell types (e.g.,
295 monocytes, macrophages) exhibit biased expression. CD36 mediates the formation of giant cells, but does
296 not facilitate osteoclast fusion (25). Our data further confirm that $CD11B^{+}CD36^{+}$ cells do not form
297 osteoclasts.

298 Global deletion of *Cd36* (i.e., *Cd36*$^{-/-}$) resulted in conflicting effects on bone mass. In the first published
299 study, male and female 1- to 6-month-old *Cd36*$^{-/-}$ mice demonstrated reduced vertebral and femoral
300 cortical bone mass characterized by diminished bone formation (34). No changes in markers of resorption
301 were noted (34). Furthermore, in vitro osteoblastogenesis from bone marrow stromal cells was
302 diminished, though the impact of myeloid cell *Cd36* deletion in these cultures could be a confounding
303 factor. Conversely, a later study reported increased vertebral and femoral cortical BV/TV in female 12-

304 week-old *Cd36*$^{-/-}$ mice, with no detection of CD36 expression by mature osteoclasts or osteoblasts (35).
305 Given these conflicting results using *Cd36* global knockout mice, an examination of the role of *Cd36*
306 specifically within monocyte/macrophage-lineage cells during bone remodeling and regeneration is
307 warranted as understanding the role of *Cd36* in bone biology would offer potential therapeutic targets for
308 managing bone-related diseases and improving skeletal health.

309 Our scRNA-Seq data demonstrated enrichment of secreted factors (e.g., Wnts, Bmps) by aged myeloid
310 cells within our clusters of interest. Coupled with decreased endosteal perimeter, we speculated that
311 CD11B^{+}CD36^{+} cells may limit resorption at endosteal surfaces. Wnt signaling limits osteoclastogenesis
312 (36). Likewise, canonical Wnt signaling promotes expression of OPG by osteoblasts, leading to diminished
313 osteoclastogenesis (37). In contrast, little is known about production of Wnt ligands by other cell types
314 involved in bone remodeling and how this impacts cortical bone resorption. In fact, studies suggest that
315 osteoclasts and bone forming osteoblasts may not be present at sites of bone remodeling at the same
316 time (38-40), particularly at the endosteal surface. Likewise, age disrupts the temporal and spatial
317 processes of resorption and formation. Our studies point to CD11D^{+}CD36^{+} cells as targets to limit age-
318 associated cortical bone loss. In future studies, we will determine factors produced CD11B^{+} CD36^{+} cells
319 that limit age-associated osteoclastogenesis and bone resorption.

320 Our study has several limitations. We did not assess possible contributions of splenic cells to our
321 phenotype. Studies have shown that osteoclast progenitors from the spleen can migrate to bone and
322 participate in bone remodeling and repair (28, 31, 33). We did not observe significant expression of X-
323 linked gene within the bone marrow of males reconstituted with female bone marrow or splenomegaly;
324 nonetheless, we cannot completely rule out the contribution of these cells within our study. Although we
325 speculate that CD11B^{+}CD36^{+} cells are not osteomorphs based on their inability to support
326 osteoclastogenesis in vitro, we do not know if this is true in vivo. Our definition of aged mice does not
327 strictly fit the well-accepted definition (e.g., older than one year). We wanted to uncover mechanisms of

328 age-associated bone loss independent of reproductive status to reflect what may be initiating events in
329 the aging process as both men and women begin to lose bone mass starting in the third decade of life.

330 **MATERIALS AND METHODS**

331 *Animal procurement and housing*

332 The Jackson Laboratory provided male and female C57Bl6/J mice (strain #000664, Bar Harbor, ME, USA)
333 aged to either 6- or 38-weeks old at time of purchase. Mice were acclimated to housing conditions for
334 two weeks prior to experimentation. All animal research was conducted according to guidelines provided
335 by the National Institutes of Health and the Institute of Laboratory Animal Resources, National Research
336 Council. The University of Minnesota Institutional Animal Care and Use Committee approved all animal
337 studies.

338 *T Cell Depletion of Whole Bone Marrow*

339 Male and female 8- or 40-week-old mice were euthanized by CO_2 asphyxiation. The femora and tibiae
340 were collected and connective tissue was removed. Bone epiphyses were removed and the marrow cavity
341 was flushed with sterile PBS. Whole bone marrow suspensions from age-matched mice were pooled and
342 pelleted at 1000 rpm for five minutes. Cell pellets were then suspended in 1X RBC lysis buffer (#00-4333-
343 57, ThermoFisher Scietific, Waltham, MA, USA) and incubated for five minutes. Cells were pelleted at 1000
344 rpm and suspended in MACS buffer (0.5% bovine serum albumin, 2mM EDTA, phosphate buffered saline)
345 by diluting MACS BSA stock solution (Miletnyi Biotech, Bergisch Gladbach, North Rhine-
346 Westphalia, Germany, #130-091-376) 1:20 with autoMACS rinsing solution (Miltenyi Biotech, #130-091-
347 222,) to a density of $0.2x10^6$ cells/µl. Cell suspensions were then incubated with 1 µl PE-conjugated anti-
348 CD8 and anti-CD3 antibodies per $1x10^7$ nucleated cells for 20 minutes in the dark at 4C. Cells were then
349 washed with MACS buffer, pelleted and suspended at a density of $1.25x10^6$ cells/µl in MACS buffer. Anti-
350 PE microbeads (20 µl/$10x10^6$ cells, Miltenyi Biotech, #130-048-801) were added and cells were incubated
351 at 4C for 20 minutes in the dark. Cells were then washed pelleted and applied to an LS column (#130-042-

352 401, Miltenyi Biotech) placed in a MidiMACS Separator magnet (Miltenyi Biotec, #130-042-301h). Eluted
353 $CD8^-/CD3^-$ bone marrow cells were pelleted and suspended in PBS at a density of $50x10^6$ cells/ml.
354 *Irradiation and bone marrow reconstitution*
355 Six-week-old (e.g., young) male mice (n=34) were lethally irradiated using and X-ray irradiator via two
356 successive does of 500 rads separated by a period of four hours. Two hours after completion of irradiation,
357 mice were reconstituted via a 200 µl tail vein injection of $10x10^6$ T cell-depleted whole bone marrow cells
358 suspended in PBS derived from either 6-week-old males (n=10), 6-week-old females (n=8), 40-week-old
359 males (n=8), or 40-week-old females (n=8). Following bone marrow reconstitution, mice were housed in
360 autoclaved cages and were administered 15 µg polymixin B sulfate and 40 µg/ml neomycin sulfate in their
361 drinking water for two weeks. Mice were aged an additional 16 weeks (e.g., 24-weeks-old) and then
362 euthanized for analyses.
363 *Micro-computed tomography*
364 Right femora collected from 24-week-old chimeric mice and non-irradiated 24-week old males were fixed
365 in 10% neutral buffered formalin for 48 hours, wrapped in gauze, and placed in 1.5mL screw-cap tubes
366 filled with 70% ethanol. Scanning was performed using the XT H 225 micro-computed tomography (micro-
367 CT) machine (Nikon Metrology Inc., Brighton, MI, USA) set to 120kV, 61µA, 720 projections at two frames
368 per projection with an integration time of 708 milliseconds as previously described (41). Scans were done
369 at an isometric voxel size of 7.11 µm with a 1mm aluminum filter, 17 minutes per scan. Each scan volume
370 was reconstructed using CT Pro 3D (Nikon metrology, Inc., Brighton, MI, USA). Reconstructions were
371 converted to bitmap datasets using VGStudio MAX 3.2 (Volume Graphics GmbH, Heidelberg, Germany).
372 Scans were reoriented via DataViewer (SkyScan, Bruker micro-CT, Belgium) to create a new bitmap
373 dataset for consistent analysis. From these data, representative transverse slices were selected for
374 qualitative analysis. Morphometric analysis was performed using SkyScan CT-Analyzer (CTAn, Bruker
375 micro-CT). Bruker's instructions and guidelines for analysis within the field was followed throughout

376 analysis (41). 3D Analysis of trabecular bone was performed in the distal metaphysis 0.7 mm proximal to
377 the growth plate and extending 1.5 mm proximally toward the bone diaphysis. For the bone cortex, 2D
378 analysis occurred in a 0.5 mm section within the mid-diaphysis defined as 4 mm from the growth plate.
379 Regions of interest were set by automated contouring for the trabecular and cortical ranges, with some
380 manual editing when necessary. Binary selection of all samples resulted in two separate global thresholds
381 used to separate bone from surrounding tissue within the trabecular and cortical regions of interest.
382 Parameters measured for trabecular bone include bone volume per total volume (BV/TV), bone surface
383 per total volume (BS/TV), bone surface per bone volume (BS/BV) trabecular thickness, number, and
384 spacing (Tb.Th, Tb.N, Tb.Sp), and connective density (Conn.D). Cortical parameters measured were BV/TV,
385 periosteal and endosteal perimeter (pM), as well as cortical thickness (Ct.Th).

386 *$CD11B^+$ magnetic assisted cell sorting*

387 Bone marrow cells were flushed from the femora and tibiae of 6-month-old chimeric mice from each
388 group or from 8- and 40-week-old male and female C57Bl6/J mice. Whole bone marrow suspensions
389 resulting from each mouse were pelleted at 1000 rpm for five minutes. Cell pellets were then suspended
390 in 1X RBC lysis buffer and incubated for five minutes. Cells were pelleted at 1000 rpm and suspended in
391 MACS buffer to a density of $0.11x10^6$ cells/µl. Nucleated cells were then incubated with 10 µl CD11B
392 microbeads (Miltenyi Biotech, #130-126-725) per $1x10^7$ cells for 10 minutes at 4C. Cell suspensions were
393 then brought to a total volume of 500 µl with MACS buffer and applied to an equilibrated LS column placed
394 in a MidiMACS Separator magnet. Columns were then washed three times with MACS buffer and removed
395 from the magnet. $CD11B^+$ cells were eluted from the column with 5 ml MACS buffer. Cells were then
396 enumerated and used for subsequent scRNA-Seq analyses.

397 *Single cell RNA-sequencing*

398 CD11B+ cells from chimeric mice in each group or 8- and 40-week-old male and female C57Bl6/J mice
399 were isolated via MACS as described above. Single cell cDNA libraries from each sample were the

400 prepared using Chromium Single cell 3' Reagent v3 Kits (10× Genomics, Pleasanton, CA, USA) according to
401 the manufacturer's protocol. Each single-cell suspension was mixed with primers, enzymes, and gel beads
402 containing barcode information and then loaded on a Chromium Single Cell Controller (10× Genomics) to
403 generate single-cell gel beads in emulsions (GEMs). Each gel bead was bonded to one cell and encased
404 within oil surfactant. After generating the GEMs, reverse transcription was performed using barcoded full-
405 length cDNA followed by the disruption of emulsions using the recovery agent and cDNA clean up with
406 DynaBeads MyOne Silane Beads (ThermoFisher Scientific, #37002D). cDNA was then amplified by PCR
407 with an appropriate number of cycles and thermal conditions that depended on the recovery cells.
408 Subsequently, the amplified cDNA was fragmented, end-repaired, A-tailed, ligated to an index adaptor,
409 and subjected to library amplification. Quality of amplified cDNA was assessed using an Agilent
410 Bioanalyzer prior to high-throughput sequencing. Following quality control, the cDNA libraries were
411 sequenced on an Illumina NovaSeq 6000 sequencer. The Genomics Core at the University of Minnesota
412 performed library construction and sequencing.

413 *Single Cell Bioinformatic Analyses*

414 10× Genomics Cell Ranger software (version 6.0.0) was used to process the raw scRNA-seq data in
415 accordance with the guidelines specified by the manufacturer. Cell Ranger software (2020-A, 10×
416 Genomics Cell Ranger Count v7.0.1) was used to demultiplex the raw base call (BCL) files produced by the
417 Illumina NovaSeq 6000 sequencer. Next, Cell Ranger was used to count the unique molecular identifiers
418 (UMI) and barcodes and align fastq files to the mouse reference genome (GRCm39). Quality assurance
419 and subsequent studies were then performed on the feature-barcode matrices created by Cell Ranger.
420 The study was filtered to exclude cells with outlier status, aberrant gene detection rates (<500 and
421 >5,000), and high mitochondrial transcript level (>8%, a sign of cellular stress). Cells were then organized
422 into an ideal number of clusters for de novo cell type discovery. Then, using uniform manifold
423 approximation and projection (UMAP), a non-linear dimensional reduction was carried out, enabling for

424 the identification and visualization of different cell clusters. Data integration was performed to compare
425 between samples.

426 *CD11B$^+$CD36$^+$ Cell Isolation*

427 Whole bone marrow was flushed from the hind limbs of 6-8-week-old male and female C57Bl6/J mice
428 (n=3 per sex) and red blood cells were lysed with 1X RBC lysis buffer as described above. Nucleated cells
429 from whole bone marrow were pelleted at 1000 rpm for 5 minutes, and the supernatant was removed
430 and discarded. Nucleated cells were divided into two subsets, one for isolation of all CD11B$^+$ cells within
431 the bone marrow and the other for isolation of CD11B$^+$/CD36$^-$ and CD11B$^+$/CD36$^+$ cells. Cells were counted
432 and pelleted at 1000 rpm. Nucleated cells within the pellet were suspended in 100 µl MACS Buffer per
433 1x10^7. For isolation of CD36$^+$ cells, cells were then incubated with Allophycocyanin (APC)-conjugated anti-
434 CD36 (10 µl per 1x10^7 cells, Miltenyi Biotech, #130-122-085) antibodies for 10 minutes at 4C. Cells were
435 pelleted, washed, suspended in 1X MACS buffer (80 µl per 1x10^7 cells) and incubated with anti-APC
436 microbeads (20 µl per 1x10^7 cells, Miltenyi Biotech, #130-090-855) for 15 minutes at 4C. Cells were
437 washed and then suspended in 500 µl MACS buffer. An LS MACS separation column was placed within
438 the magnetic field of a MACS Separator magnet and the column was equilibrated with 3 ml MACS buffer.
439 Following equilibration, anti-APC microbead-labeled cells were applied to the LS column. The column was
440 washed 3X with 3 ml MACS buffer. Unbound cells were used to isolate CD11B$^+$CD36$^-$ cells. To isolate APC-
441 labeled cells, the column was removed from the magnet and cells were flushed from the column with 5
442 ml 1X MACS buffer. Eluted cells were then pelleted at 1000 rpm for 5 minutes, and the supernatant was
443 removed and discarded. To isolate CD11B$^+$ cells from each of the three fractions (e.g., whole bone marrow,
444 CD36$^-$ cells, and CD36$^+$ cells), cells were then suspended in 100 µl 1X MACS Buffer per 1x10^7 cells and
445 incubated with phycoerythrin (PE)-conjugated anti-CD11B (10 µl per 1x10^7 cells, Miltenyi Biotech, #130-
446 113-235) for 10 minutes at 4C. Cells were washed, suspended in MACS buffer (80 µl per 1x10^7 cells), and
447 incubated with anti-PE microbeads (20 µl per 1x10^7 cells, Miltenyi Biotech, #130-048-801) for 15 minutes

448 at 4C. Magnetic sorting for PE-labeled cells was accomplished as described above. To validate effective
449 sorting of $CD36^+CD11B^+$ cells via MACS, flow cytometry was performed (n=3). For flow cytometry analysis,
450 we prepared single stained controls and double stained sample with unsorted nucleated cells with PE-
451 conjugated anti-CD11B, APC-conjugated anti-CD36, or co-stained with anti-CD11B and anti-CD36
452 antibodies ($1x10^6$ cells per condition), respectively. Data were acquired on a BD LSR II (H1010) and
453 analyses were performed using BD FACSDiva™ software.

454 *Culture of $CD36^+CD11B^+$ cells*

455 MACS sorted $CD11B^+$, $CD11B^+/CD36^-$ and $CD36^+/CD11B^+$ cells were isolated via MACS and cultured at a
456 density of $0.26x10^6$ per cm^2 in α-Minimal Essential Medium supplemented with 50 ng/ml recombinant
457 mouse macrophage-colony stimulating factor (M-CSF) (#416-ML, R&D Systems, Minneapolis, MN, USA).
458 Cells were maintained in culture and supplemented with M-CSF for 7 days or until adherent. Medium
459 conditioned by each cell fraction was then collected, filtered with a 70 µm filter to remove cellular debris,
460 and stored at -80C before subsequent analyses. Cells were lysed in TriZol reagent (ThermoFisher Scientific,
461 #15596018) for gene expression analyses. For osteoclastogenesis experiments, cells from each fraction
462 were plated at a density of $0.4x10^6/cm^2$ in αMEM supplemented with 100 ng/ml RANKL (R&D Systems,
463 #462-TR-010) and 50 ng/ml M-CSF. Cells were refed with αMEM supplemented with RANKL and M-CSF
464 every other day for seven days, fixed with 10% neutral buffered formalin, and TRAP stained using the
465 Leukocyte Acid Phosphatase (TRAP) kit (Sigma-Aldrich, #387A-1KT).

466 *RNA Isolation and Semi-quantitative RT-PCR*

467 Total RNA was extracted from human macrophages using TRIzol and chloroform. Reverse transcription
468 using the iScript™ Reverse Transcription Supermix (Biorad, #1708841) using 1 µg of total RNA was used to
469 generate cDNAs. Gene expression was then assessed via real-time PCR using gene-specific primers listed
470 in Table 1. Fold changes in gene expression for each sample were calculated using the $2^{-\Delta\Delta Ct}$ method

471 relative to control after normalization of gene-specific C_t values to Ywhaz C_t values (24, 42). Shown are
472 averaged data from three independent replicate experiments derived from female cultured cells.

473 **Table 1. Gene specific primers used for semi-quantitative RT-PCR.**

Target	Forward Primer	Reverse Primer
Wnt3a	5'-TGTTCTGGACAAAGCCACCC-3'	5'-AATGTCCTCACTACAGCCGC-3'
Wnt6	5'-ACTGGGGGTTCGAGAATGTC-3'	5'-TCTCTCGGATGTCCTGCTGC-3'
Wnt10b	5'-ACGCCGGGGAAGCGG-3'	5'-AGTCAGTCAGCGCCTCCAG-3'
Bmp1	5'-TGGCCATATCCAGTCTCCCA-3'	5'-TGTCGTGACGCTCAATCTCA-3'
Bmp2	5'-CTGCGGTCTCCTAAAGGTCG-3'	5'-ATGCTGAGCAGCCTCAACTC-3'

474

475 *Cortical Bone Defect Generation*

476 Single-cortex, fully stabilized, mid-diaphysis femoral defects were generated in the right femur as
477 previously described (24, 43). Mice in all experimental groups were given Buprenorphine SR provided
478 perioperatively at 0.5 mg/kg given 2-4 hours before surgery via subcutaneous injection. Mice were then
479 anesthetized with isoflurane and prepared for aseptic surgery. A small incision was made in the skin
480 overlying the right hamstring and the femoral bone shaft was exposed by blunt dissection of the
481 underlying muscle. A 0.7 mm diameter steel burr drill bit (#19007-07, Fine Science Tools, Foster City, CA)
482 and an electric drill was used to induce a single-cortex defect in the mid-diaphysis of the femur. Defects
483 were immediately irrigated with 1 ml sterile saline followed by incision closure. Mice were sacrificed by
484 carbon dioxide inhalation on postoperative day 14.

485 *Immunohistochemistry (IHC) and TRAP Staining*

486 Tibiae from 24-week-old female mice were collected, fixed in 10% neutral buffered formalin for 24 hours
487 and then stored in 70% ethanol. Following decalcification in 15% EDTA for 14 days, tissues were paraffin
488 embedded and 7 micron sections were collected. IHC staining was performed with antibodies directed to
489 CD36 (#HPA002018, Sigma-Aldrich), or an irrelevant control. Detection was accomplished using the

490 Mouse and Rabbit Specific HRP/DAB (ABC) Detection IHC Kit (#ab64264, Abcam, Cabmbridge, UK).
491 Sections were the TRAP stained and then counterstained with Fast Green as previously described (42).

492 *Measurements of proliferation and osteoblastogenesis*

493 ST2 cells were cultured at a density of XXX cells/cm2 in $CD11B^+$, $CD11B^+/CD36^-$ or $CD11B^+/CD36^+$
494 conditioned medium for 24 hours. MSC proliferation was then determined using a Cck8 assay (Cell
495 Counting Kit, Sigma Aldrich, #96992-100TESTS-F). To assess MSC migration, transwell assays were
496 performed using Corning Costar transwell assay cell culture inserts (Sigma Aldrich, #CLS3464-12EA).
497 Before starting the assay, the transwell were equilibrated over night with MEM (no FBS). Next day, ST2
498 cells were trypsinized and collected in 0.2% FBS containing MEM. A total of $2x10^4$ cells were seeded into
499 the upper chamber of the transwell inserts. The lower chamber was filled with an equal mixture of
500 conditioned medium and MEM (10% FBS). Then, the plate was incubated for 18hrs to allow migration.
501 Following incubation, the plate was taken out and the media was removed. The insert was washed with
502 1x PBS two times. The non-migrated cells were carefully removed from the upper side of the membrane
503 using cotton swab and the migrated cells on the other side of the membrane was fixed with 100%
504 methanol, for 5 min at room temperature and stained with Giemsa stain for 10min. Excess stain was
505 removed by washing the chamber with distilled water and then air drying The membrane was carefully
506 cut out using a scalpel blade and placed on slide. The membrane was mounted on the slide using
507 VECTASHIELD® Antifade Mounting Medium with DAPI. Cells were visualized under the fluorescent
508 microscope, and five random fields per insert were counted using Image J.

509 *Western Blotting*

510 Cell lysates were collected in a buffered SDS solution (0.1% glycerol, 0.01% SDS, 0.1 m Tris, pH 6.8) on ice.
511 Total protein concentrations were obtained with the Bio-Rad D_C assay (Bio-Rad). Proteins (20 µg) were
512 then resolved by SDS-PAGE and transferred to a polyvinylidene difluoride membrane. Western blotting
513 was performed with antibodies (1:2000 dilution) for WNT6 (Thermo Fisher Scientific, #24201-1-AP), Active

514 β-catenin (Millipore, #05-665-25UG), β-catenin (BD Biosciences, #610153), TCF1/7 (Cell Signaling
515 Technology, 2203T), phospho-JNK (Cell Signaling Technology, #4668T), JNK (Cell Signaling Technology,
516 #9252T), NFAT1 (Cell Signaling Technology, #4389S), Histone 3 (Millipore, #05-928), and corresponding
517 secondary antibodies conjugated to horseradish peroxidase (HRP) (Cell Signaling Technology). Antibody
518 binding was detected with the Supersignal West Femto Chemiluminescent Substrate (Pierce
519 Biotechnology, Rockford, IL). Shown are data from averaged from three males, but studies were
520 performed in females (n=3 per group) in three independent replicate experiments, each containing six
521 pooled replicate wells per group.

522 **CONFLICTS OF INTEREST**

523 The authors declare no conflict of interest.

524 **ACKNOWLEDGEMENTS**

525 The authors would like to thank the support from the Comparative Pathology Shared Resource, the
526 Minnesota Dental Research Center for Biomaterials and Biomechanics, and technical assistance from Mr.
527 David HH Molstad. This work was made possible by research grants from the National Institute for
528 Musculoskeletal, Arthritis, and Skin Diseases (R21AR084530), a seed grant from the UMN BIRCWH award
529 (HD055887), and the University of Minnesota Board of Regents. These contents are solely the
530 responsibility of the authors and do not necessarily represent the official views of the funding
531 organizations. The study was conducted according to the guidelines of the University of Minnesota
532 Institutional Animal Care and Use Committee (#2007-38247A approved on 08 August 2020). All data are
533 contained within this manuscript and are available from the corresponding author upon reasonable
534 request.

535 **REFERENCES**

536 1. Chevalley T, Rizzoli R. Acquisition of peak bone mass. Best Pract Res Clin Endocrinol Metab.
537 2022;36(2):101616.
538 2. Demontiero O, Vidal C, Duque G. Aging and bone loss: new insights for the clinician. Ther Adv
539 Musculoskelet Dis. 2012;4(2):61-76.
540 3. Sfeir JG, Drake MT, Khosla S, Farr JN. Skeletal Aging. Mayo Clin Proc. 2022;97(6):1194-208.
541 4. Wright NC, Looker AC, Saag KG, Curtis JR, Delzell ES, Randall S, et al. The recent prevalence of
542 osteoporosis and low bone mass in the United States based on bone mineral density at the femoral neck
543 or lumbar spine. J Bone Miner Res. 2014;29(11):2520-6.
544 5. Kannus P, Parkkari J, Niemi S, Palvanen M. Epidemiology of osteoporotic ankle fractures in elderly
545 persons in Finland. Ann Intern Med. 1996;125(12):975-8.
546 6. Leibson CL, Tosteson AN, Gabriel SE, Ransom JE, Melton LJ. Mortality, disability, and nursing home
547 use for persons with and without hip fracture: a population-based study. J Am Geriatr Soc.
548 2002;50(10):1644-50.
549 7. Magaziner J, Lydick E, Hawkes W, Fox KM, Zimmerman SI, Epstein RS, et al. Excess mortality
550 attributable to hip fracture in white women aged 70 years and older. Am J Public Health.
551 1997;87(10):1630-6.
552 8. Magaziner J, Simonsick EM, Kashner TM, Hebel JR, Kenzora JE. Predictors of functional recovery
553 one year following hospital discharge for hip fracture: a prospective study. J Gerontol. 1990;45(3):M101-
554 7.
555 9. Riggs BL, Melton LJ, 3rd. The worldwide problem of osteoporosis: insights afforded by
556 epidemiology. Bone. 1995;17(5 Suppl):505S-11S.
557 10. Clarke B. Normal bone anatomy and physiology. Clin J Am Soc Nephrol. 2008;3 Suppl 3(Suppl
558 3):S131-9.
559 11. Ramchand SK, Seeman E. The Influence of Cortical Porosity on the Strength of Bone During Growth
560 and Advancing Age. Curr Osteoporos Rep. 2018;16(5):561-72.
561 12. Cosman F, Crittenden DB, Ferrari S, Khan A, Lane NE, Lippuner K, et al. FRAME Study: The
562 Foundation Effect of Building Bone With 1 Year of Romosozumab Leads to Continued Lower Fracture Risk
563 After Transition to Denosumab. J Bone Miner Res. 2018;33(7):1219-26.
564 13. Graeff C, Campbell GM, Pena J, Borggrefe J, Padhi D, Kaufman A, et al. Administration of
565 romosozumab improves vertebral trabecular and cortical bone as assessed with quantitative computed
566 tomography and finite element analysis. Bone. 2015;81:364-9.
567 14. Weivoda MM, Bradley EW. Macrophages and Bone Remodeling. J Bone Miner Res.
568 2023;38(3):359-69.
569 15. Sims NA, Martin TJ. Osteoclasts Provide Coupling Signals to Osteoblast Lineage Cells Through
570 Multiple Mechanisms. Annu Rev Physiol. 2020;82:507-29.
571 16. Andreasen CM, El-Masri BM, MacDonald B, Laursen KS, Nielsen MH, Thomsen JS, et al. Local
572 coordination between intracortical bone remodeling and vascular development in human juvenile bone.
573 Bone. 2023;173:116787.
574 17. Liu B, Salgado OC, Singh S, Hippen KL, Maynard JC, Burlingame AL, et al. The lineage stability and
575 suppressive program of regulatory T cells require protein O-GlcNAcylation. Nat Commun. 2019;10(1):354.
576 18. Wang H, Breed ER, Lee YJ, Qian LJ, Jameson SC, Hogquist KA. Myeloid cells activate iNKT cells to
577 produce IL-4 in the thymic medulla. Proc Natl Acad Sci U S A. 2019;116(44):22262-8.
578 19. Wang H, Hogquist KA. CCR7 defines a precursor for murine iNKT cells in thymus and periphery.
579 Elife. 2018;7.
580 20. Faltusova K, Chen CL, Heizer T, Bajecny M, Szikszai K, Paral P, et al. Altered Erythro-Myeloid
581 Progenitor Cells Are Highly Expanded in Intensively Regenerating Hematopoiesis. Front Cell Dev Biol.
582 2020;8:98.

583 21. Mohamad SF, Gunawan A, Blosser R, Childress P, Aguilar-Perez A, Ghosh J, et al. Neonatal
584 Osteomacs and Bone Marrow Macrophages Differ in Phenotypic Marker Expression and Function. J Bone
585 Miner Res. 2021;36(8):1580-93.
586 22. McDonald MM, Khoo WH, Ng PY, Xiao Y, Zamerli J, Thatcher P, et al. Osteoclasts recycle via
587 osteomorphs during RANKL-stimulated bone resorption. Cell. 2021;184(5):1330-47 e13.
588 23. Isojima T, Sims NA. Cortical bone development, maintenance and porosity: genetic alterations in
589 humans and mice influencing chondrocytes, osteoclasts, osteoblasts and osteocytes. Cell Mol Life Sci.
590 2021;78(15):5755-73.
591 24. Molstad DHH, Zars E, Norton A, Mansky KC, Westendorf JJ, Bradley EW. Hdac3 deletion in myeloid
592 progenitor cells enhances bone healing in females and limits osteoclast fusion via Pmepa1. Sci Rep.
593 2020;10(1):21804.
594 25. Helming L, Winter J, Gordon S. The scavenger receptor CD36 plays a role in cytokine-induced
595 macrophage fusion. J Cell Sci. 2009;122(Pt 4):453-9.
596 26. Ambrosi TH, Marecic O, McArdle A, Sinha R, Gulati GS, Tong X, et al. Aged skeletal stem cells
597 generate an inflammatory degenerative niche. Nature. 2021;597(7875):256-62.
598 27. Ucer S, Iyer S, Kim HN, Han L, Rutlen C, Allison K, et al. The Effects of Aging and Sex Steroid
599 Deficiency on the Murine Skeleton Are Independent and Mechanistically Distinct. J Bone Miner Res.
600 2017;32(3):560-74.
601 28. Yahara Y, Ma X, Gracia L, Alman BA. Monocyte/Macrophage Lineage Cells From Fetal
602 Erythromyeloid Progenitors Orchestrate Bone Remodeling and Repair. Front Cell Dev Biol. 2021;9:622035.
603 29. Askmyr MK, Fasth A, Richter J. Towards a better understanding and new therapeutics of
604 osteopetrosis. Br J Haematol. 2008;140(6):597-609.
605 30. Jacome-Galarza CE, Percin GI, Muller JT, Mass E, Lazarov T, Eitler J, et al. Developmental origin,
606 functional maintenance and genetic rescue of osteoclasts. Nature. 2019;568(7753):541-5.
607 31. Novak S, Roeder E, Kalinowski J, Jastrzebski S, Aguila HL, Lee SK, et al. Osteoclasts Derive
608 Predominantly from Bone Marrow-Resident CX3CR1(+) Precursor Cells in Homeostasis, whereas
609 Circulating CX3CR1(+) Cells Contribute to Osteoclast Development during Fracture Repair. J Immunol.
610 2020;204(4):868-78.
611 32. Xia Y, Inoue K, Du Y, Baker SJ, Premkumar Reddy E, Greenblatt MB, et al. TGFbeta reprograms TNF
612 stimulation of macrophages towards a non-canonical pathway driving inflammatory osteoclastogenesis.
613 Nat Commun. 2022;13(1):3920.
614 33. Yahara Y, Barrientos T, Tang YJ, Puviindran V, Nadesan P, Zhang H, et al. Erythromyeloid
615 progenitors give rise to a population of osteoclasts that contribute to bone homeostasis and repair. Nat
616 Cell Biol. 2020;22(1):49-59.
617 34. Kevorkova O, Martineau C, Martin-Falstrault L, Sanchez-Dardon J, Brissette L, Moreau R. Low-
618 bone-mass phenotype of deficient mice for the cluster of differentiation 36 (CD36). PLoS One.
619 2013;8(10):e77701.
620 35. Koduru SV, Sun BH, Walker JM, Zhu M, Simpson C, Dhodapkar M, et al. The contribution of cross-
621 talk between the cell-surface proteins CD36 and CD47-TSP-1 in osteoclast formation and function. J Biol
622 Chem. 2018;293(39):15055-69.
623 36. Weivoda MM, Ruan M, Hachfeld CM, Pederson L, Howe A, Davey RA, et al. Wnt Signaling Inhibits
624 Osteoclast Differentiation by Activating Canonical and Noncanonical cAMP/PKA Pathways. J Bone Miner
625 Res. 2016;31(1):65-75.
626 37. Glass DA, 2nd, Bialek P, Ahn JD, Starbuck M, Patel MS, Clevers H, et al. Canonical Wnt signaling in
627 differentiated osteoblasts controls osteoclast differentiation. Dev Cell. 2005;8(5):751-64.
628 38. Andersen TL, Sondergaard TE, Skorzynska KE, Dagnaes-Hansen F, Plesner TL, Hauge EM, et al. A
629 physical mechanism for coupling bone resorption and formation in adult human bone. Am J Pathol.
630 2009;174(1):239-47.

631 39. Eriksen EF, Gundersen HJ, Melsen F, Mosekilde L. Reconstruction of the formative site in iliac
632 trabecular bone in 20 normal individuals employing a kinetic model for matrix and mineral apposition.
633 Metab Bone Dis Relat Res. 1984;5(5):243-52.
634 40. Lassen NE, Andersen TL, Ploen GG, Soe K, Hauge EM, Harving S, et al. Coupling of Bone Resorption
635 and Formation in Real Time: New Knowledge Gained From Human Haversian BMUs. J Bone Miner Res.
636 2017;32(7):1395-405.
637 41. Bouxsein ML, Boyd SK, Christiansen BA, Guldberg RE, Jepsen KJ, Muller R. Guidelines for
638 assessment of bone microstructure in rodents using micro-computed tomography. J Bone Miner Res.
639 2010;25(7):1468-86.
640 42. Mattson AM, Begun DL, Molstad DHH, Meyer MA, Oursler MJ, Westendorf JJ, et al. Deficiency in
641 the phosphatase PHLPP1 suppresses osteoclast-mediated bone resorption and enhances bone formation
642 in mice. J Biol Chem. 2019;294(31):11772-84.
643 43. McGee-Lawrence ME, Razidlo DF. Induction of fully stabilized cortical bone defects to study
644 intramembranous bone regeneration. Methods Mol Biol. 2015;1226:183-92.

645 **Figure Legends**

646 **Figure 1. Generation of Bone Marrow Chimeric Mice.** (A-E) Young male recipient mice were lethally
647 irradiated and reconstituted with T cell-depleted bone marrow (BM) from 1) young male, 2) aged male,
648 3) young female, or 4) aged female donor mice. Recipient mice were aged to 24-weeks for subsequent
649 analyses. (A) Experimental overview. (B) RNA was collected from BM and livers of chimeric mice in group
650 3 and expression of X- and Y-linked genes was determined via qPCR, *p<0.05, n=8. (C-E) Chimeric mice
651 in each group were collected six months post-BM transplantation. Mice were (C) photographed. (D) Body
652 and (E) spleen weight/body weight was assessed, *p<0.05. Groups: 1: young male BM, n=10; 2: aged male
653 BM, n=8, 3: young female BM, n=8; and 4: aged female BM, n=8

654 **Figure 2. Transplantation of Aged Bone Marrow Enhances Cortical Bone.** (A-G) Young male recipient mice
655 were lethally irradiated and reconstituted with T cell-depleted bone marrow (BM) from 1) young male, 2)
656 aged male, 3) young female, or 4) aged female donor mice. Recipient mice were aged to 24-weeks for
657 subsequent analyses. Non-irradiated 24-week-old males were used for comparisons. Micro-CT of the
658 femoral mid-shaft was performed to determine (A) cortical BV/TV, (B) cortical thickness, (C) endosteal
659 perimeter (Pm) and (D) reconstructions were generated. The distal femoral region was also assessed to
660 determine trabecular (E) BV/TV, (F) trabecular spacing, and (G) trabecular thickness. #p< 0.05 NI vs group

661 1, *p<0.05 vs. group 1. Groups: NI: non-irradiated control, n=10; 1: young male BM, n=10; 2: aged male
662 BM, n=8, 3: young female BM, n=8; and 4: aged female BM, n=8

663 **Figure 3. Identification of Anabolic Bone Marrow Subsets.** (A-R) Young male recipient mice were lethally
664 irradiated and reconstituted with T cell-depleted bone marrow (BM) from 1) young male or 2) aged male
665 donor mice. Recipient mice were aged to 24-weeks for subsequent analyses. $CD11B^+$ cells were collected
666 from mice in groups 1 and 2 above and scRNA-Seq was performed using 10X Genomics technology.
667 Resulting data were integrated and comparative analyses were performed. (A) UMAP 2D representation
668 of $CD11B^+$ clusters derived from recipient mice transplanted with aged and young bone marrow. (B-Q)
669 Expression of surface markers used to differentiate clusters. (R) Heatmap of top differentially expressed
670 genes from mice in group 2 vs 1 in clusters 14-16 across all clusters.

671 **Figure 4. Identification of Anabolic Bone Marrow Subsets.** (A-S) Young male recipient mice were lethally
672 irradiated and reconstituted with T cell-depleted bone marrow (BM) from 1) young female or 2) aged
673 female donor mice. Recipient mice were aged to 24-weeks for subsequent analyses. $CD11B^+$ cells were
674 collected from mice in groups 1 and 2 above and scRNA-Seq was performed using 10X Genomics
675 technology. Resulting data were integrated and comparative analyses were performed. (A) UMAP 2D
676 representation of $CD11B^+$ clusters derived from recipient mice transplanted with aged and young bone
677 marrow. (B-Q) Expression of surface markers used to differentiate clusters. (R) Heatmap of top
678 differentially expressed genes from mice in group 2 vs 1 in clusters 14-16 across all clusters.

679 **Figure 5. Single Cell RNA-Seq of $CD11B^+$ Cells from Male and Female Bone Marrow Reveals Subsets of**
680 **Aged Myeloid Cells that Express Anabolic Cytokines.** (A-H) $CD11B^+$ cells from the bone marrow of 8- or
681 40-week-old male and female mice were collected and single cell RNA-Seq was performed. (A) tSNE
682 representation of data obtained from 8-week-old males. (B) Heatmap and hierarchical clustering of
683 differentially expressed genes from clusters yielded from 8-week-old male data. (C) tSNE representation

684 of data obtained from 8-week-old females. (D) Heatmap and hierarchical clustering of differentially
685 expressed genes from clusters yielded from 8-week-old female data. (E) tSNE representation of data
686 obtained from 40-week-old males. (F) Heatmap and hierarchical clustering of differentially expressed
687 genes from clusters yielded from 40-week-old male data. (G) tSNE representation of data obtained from
688 40-week-old females. (H) Heatmap and hierarchical clustering of differentially expressed genes from
689 clusters yielded from 40-week-old female data.

690 **Figure 6. CD36$^+$ Cells Associate with Sites of Cortical Bone Regeneration, but are Not Osteoclast**
691 **Progenitors**. (A) Immunohistochemical staining for CD36 of paraffin sections from uninjured 12- and 24-
692 week-old females (left and middle panels, respectively) or cortical bone defects (right panels). Sections
693 are counterstained with TRAP (purple) and fast green (n=5/group). BM: bone marrow, CB: cortical bone,
694 OC: osteoclast (B) CD11B$^+$CD36$^-$ and CD11B$^+$CD36$^+$ BM cells were isolated and cultured in the presence of
695 RANKL and M-CSF. TRAP staining was performed on day 4 (n=3).

696 **Figure 7. CD11B$^+$CD36$^+$ Cells Promote Bone Formation.** (A) Flow cytometry. CD11b+CD36- and
697 CD11b+CD36+ cells were sorted and gene expression was evaluated by qPCR (B-F) and western blotting
698 (G), n=3, *p* values as shown. (H) Experimental design for (I-Q) Osteoprogenitor cells were treated with CM
699 for 24 hours and (I) Cck8 and (J) transwell assays were performed. Osteoprogenitor cells were treated
700 with CM for 8 weeks and Alizarin Red staining (K) was performed and quantified (L), n=3, p values as
701 shown. RNA was collected and gene expression (M-Q) was assessed by qPCR, n=3, p values as shown. (R)
702 Osteoprogenitor cells were treated with CM for 60 minutes and western blotting was performed (n=3).

703 **Figure 8. Identification of Human Bone Marrow Macrophage Subsets.** CD11B$^+$ cells were collected from
704 the BM aspirate of a 45-year-old human female and scRNA-Seq was performed using 10X Genomics
705 technology. (A) UMAP 2D representation of CD11B$^+$ clusters. (B-Q) Expression of surface markers used to
706 differentiate clusters. Violin plots of CD36 (R) and Wnt6 (S) expression.

707

Figure 1

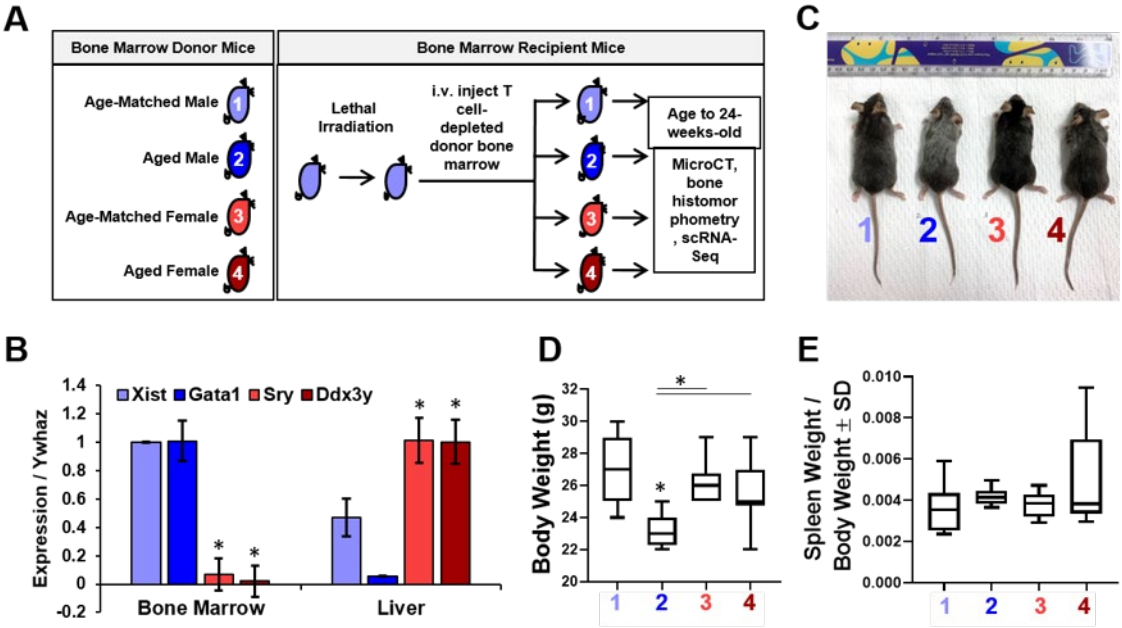
A
Bone Marrow Donor Mice
Bone Marrow Recipient Mice
Age-Matched Male
Aged Male
Age-Matched Female
Aged Female
Lethal Irradiation
i.v. inject T cell-depleted donor bone marrow
Age to 24-weeks-old
MicroCT, bone histomorphometry, scRNA-Seq
C
1
2
3
4
B
Xist
Gata1
Sry
Ddx3y
Expression / Ywhaz
Bone Marrow
Liver
D
Body Weight (g)
E
Spleen Weight / Body Weight ± SD

Figure 2

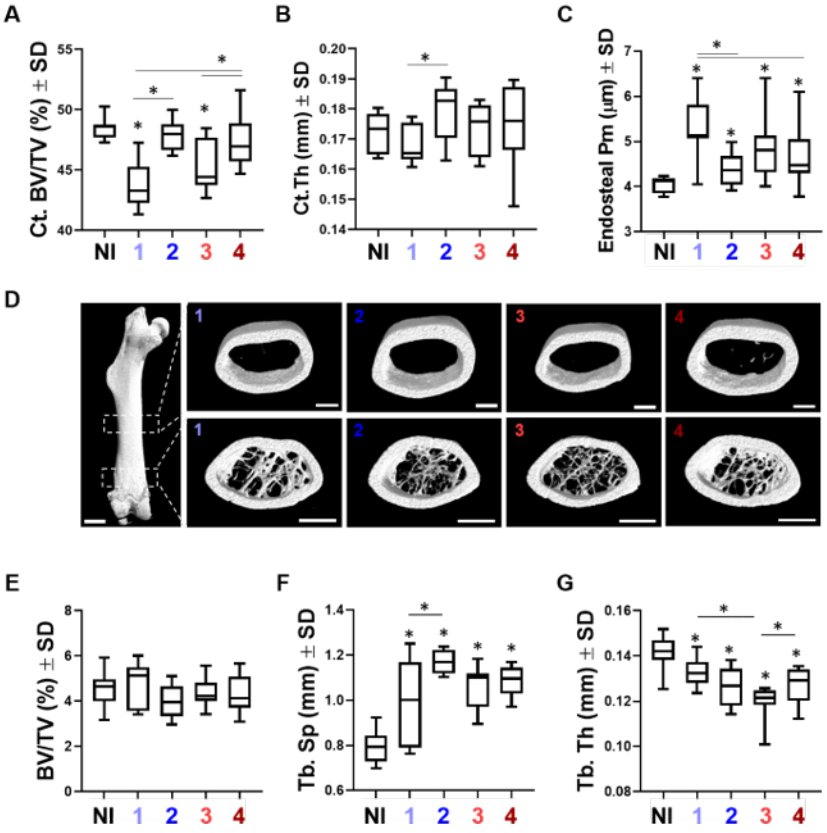
A
Ct. BV/TV (%) ± SD
B
Ct.Th (mm) ± SD
C
Endosteal Pm (µm) ± SD
D
E
BV/TV (%) ± SD
F
Tb. Sp (mm) ± SD
G
Tb. Th (mm) ± SD
NI 1 2 3 4

Figure 3

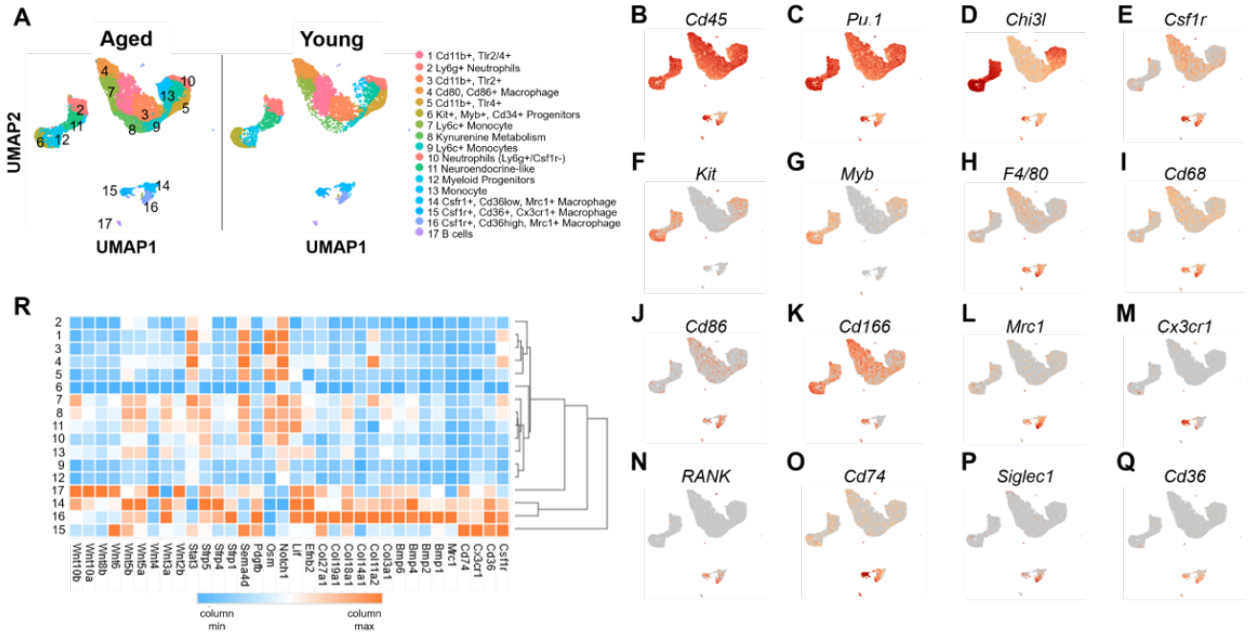
A
Aged
Young
UMAP2
UMAP1
UMAP1
1 Cd11b+, Tlr2/4+
2 Ly6g+ Neutrophils
3 Cd11b+, Tlr2+
4 Cd80, Cd86+ Macrophage
5 Cd11b+, Tlr4+
6 Kit+, Myb+, Cd34+ Progenitors
7 Ly6c+ Monocyte
8 Kynurenine Metabolism
9 Ly6c+ Monocytes
10 Neutrophils (Ly6g+/Csf1r-)
11 Neuroendocrine-like
12 Myeloid Progenitors
13 Monocyte
14 Csfr1+, Cd36low, Mrc1+ Macrophage
15 Csf1r+, Cd36+, Cx3cr1+ Macrophage
16 Csf1r+, Cd36high, Mrc1+ Macrophage
17 B cells
B Cd45
C Pu.1
D Chi3l
E Csf1r
F Kit
G Myb
H F4/80
I Cd68
J Cd86
K Cd166
L Mrc1
M Cx3cr1
N RANK
O Cd74
P Siglec1
Q Cd36
R
column min
column max

Figure 4

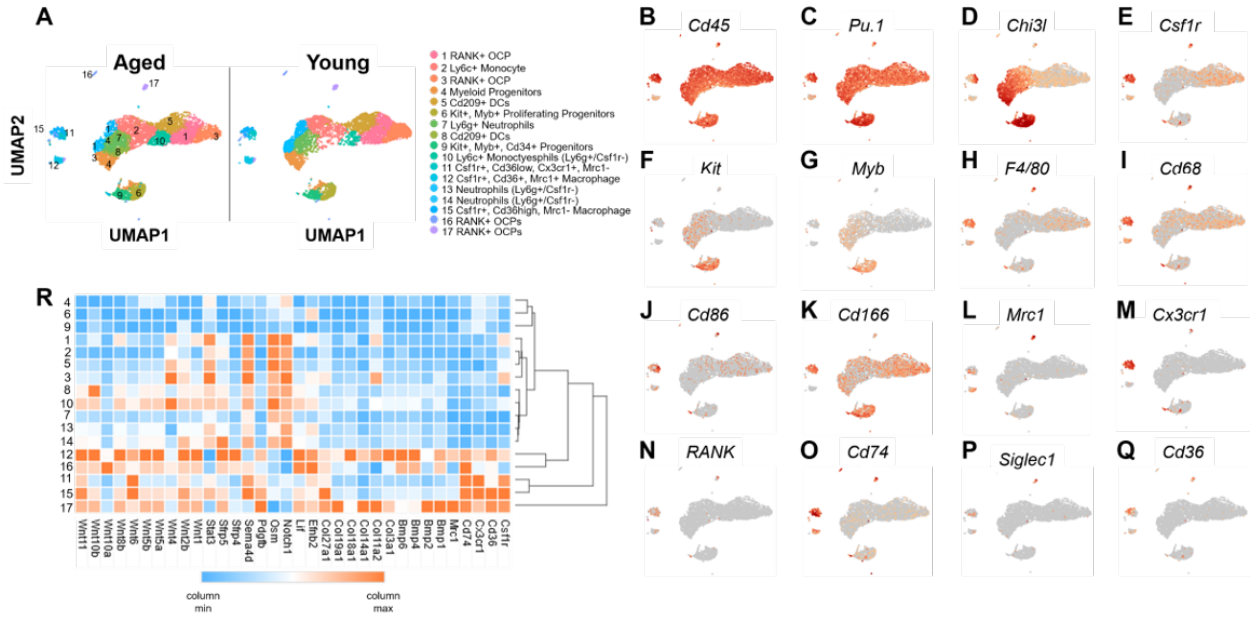
A
Aged
Young
UMAP2
UMAP1
UMAP1
1 RANK+ OCP
2 Ly6c+ Monocyte
3 RANK+ OCP
4 Myeloid Progenitors
5 Cd209+ DCs
6 Kit+, Myb+ Proliferating Progenitors
7 Ly6g+ Neutrophils
8 Cd209+ DCs
9 Kit+, Myb+, Cd34+ Progenitors
10 Ly6c+ Monoctyesphils (Ly6g+/Csf1r-)
11 Csf1r+, Cd36low, Cx3cr1+, Mrc1-
12 Csf1r+, Cd36+, Mrc1+ Macrophage
13 Neutrophils (Ly6g+/Csf1r-)
14 Neutrophils (Ly6g+/Csf1r-)
15 Csf1r+, Cd36high, Mrc1- Macrophage
16 RANK+ OCPs
17 RANK+ OCPs
B Cd45
C Pu.1
D Chi3l
E Csf1r
F Kit
G Myb
H F4/80
I Cd68
J Cd86
K Cd166
L Mrc1
M Cx3cr1
N RANK
O Cd74
P Siglec1
Q Cd36
R
Wnt11
Wnt10b
Wnt10a
Wnt8b
Wnt6
Wnt5b
Wnt5a
Wnt4
Wnt2b
Wnt1
Stat3
Stfp5
Stfp4
Sema4d
Pdgfb
Osm
Notch1
Lif
Efnb2
Col27a1
Col19a1
Col18a1
Col14a1
Col11a2
Col3a1
Bmp6
Bmp4
Bmp2
Bmp1
Mrc1
Cd74
Cx3cr1
Cd36
Csf1r
column min
column max

720

Figure 5

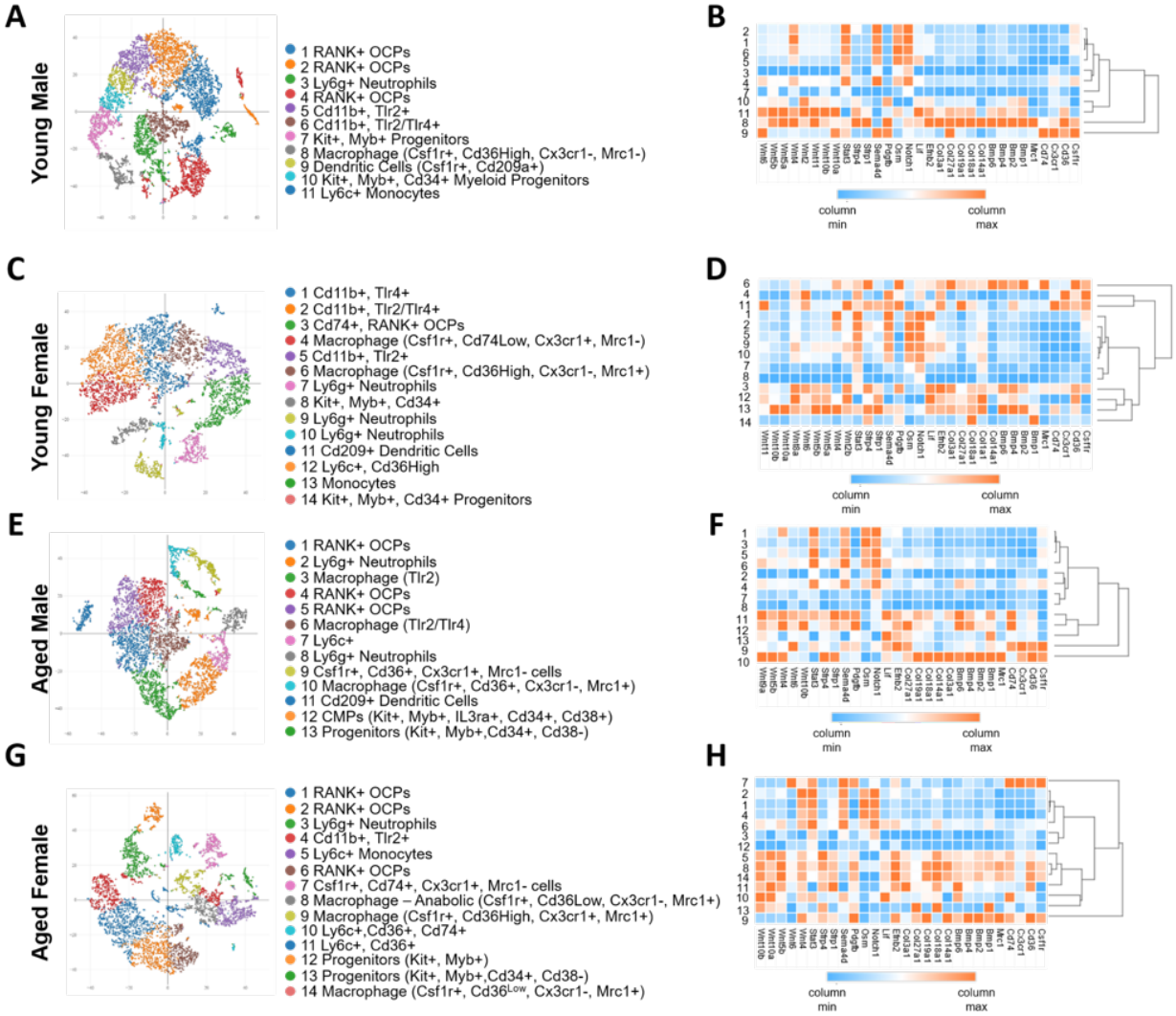

721

722

723 **Figure 6**

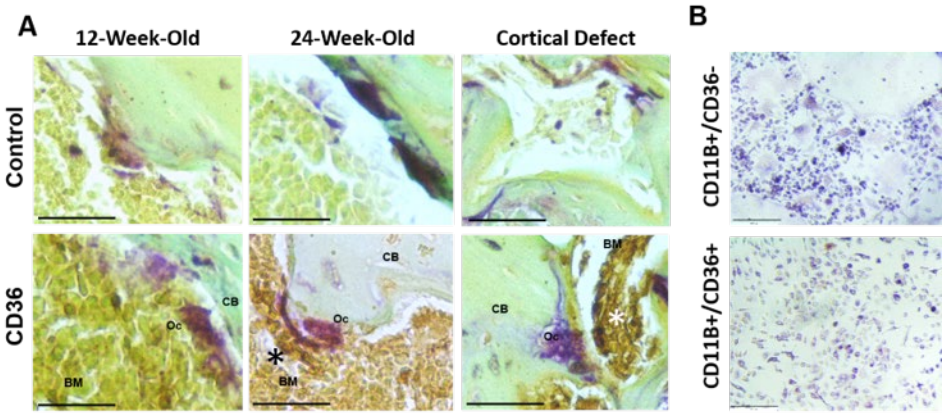

724

725

Figure 7

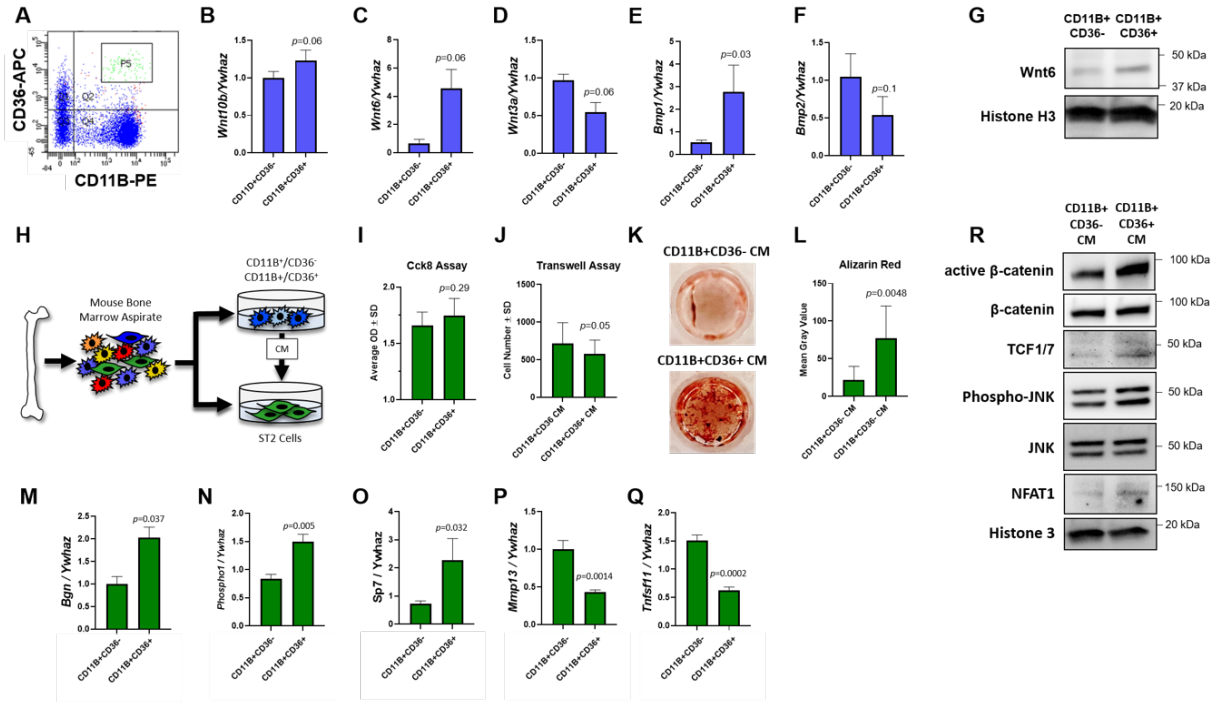
A
CD36-APC
CD11B-PE
P5
B
Wnt10b/Ywhaz
p=0.06
C
Wnt6/Ywhaz
p=0.06
D
Wnt3a/Ywhaz
p=0.06
E
Bmp1/Ywhaz
p=0.03
F
Bmp2/Ywhaz
p=0.1
CD11B+CD36-
CD11B+CD36+
G
CD11B+ CD36-
CD11B+ CD36+
Wnt6
Histone H3
50 kDa
37 kDa
20 kDa
H
Mouse Bone Marrow Aspirate
CD11B+/CD36-
CD11B+/CD36+
CM
ST2 Cells
I
Cck8 Assay
Average OD ± SD
p=0.29
J
Transwell Assay
Cell Number ± SD
p=0.05
CD11B+CD36 CM
CD11B+CD36+ CM
K
CD11B+CD36- CM
CD11B+CD36+ CM
L
Alizarin Red
Mean Gray Value
p=0.0048
CD11B+CD36- CM
CD11B+CD36+ CM
R
CD11B+ CD36- CM
CD11B+ CD36+ CM
active β-catenin
β-catenin
TCF1/7
Phospho-JNK
JNK
NFAT1
Histone 3
100 kDa
100 kDa
50 kDa
50 kDa
50 kDa
150 kDa
20 kDa
M
Bgn / Ywhaz
p=0.037
N
Phospho1 / Ywhaz
p=0.005
O
Sp7 / Ywhaz
p=0.032
P
Mmp13 / Ywhaz
p=0.0014
Q
Tnfsf11 / Ywhaz
p=0.0002

Figure 8

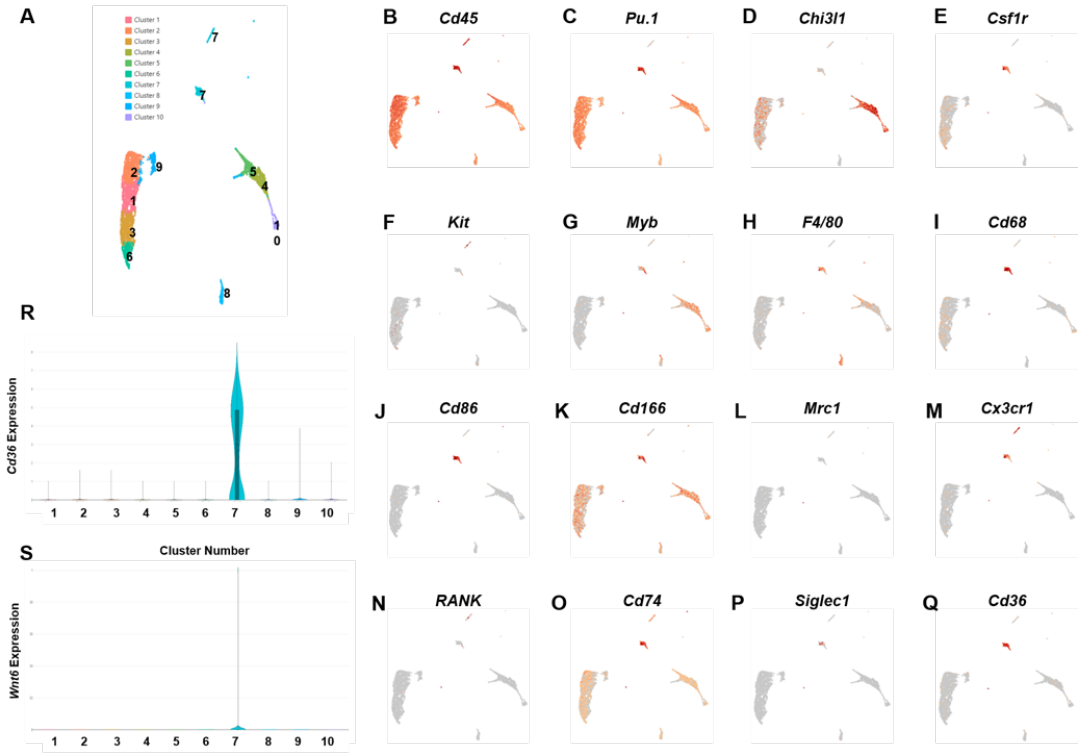
A
B Cd45
C Pu.1
D Chi3l1
E Csf1r
F Kit
G Myb
H F4/80
I Cd68
J Cd86
K Cd166
L Mrc1
M Cx3cr1
N RANK
O Cd74
P Siglec1
Q Cd36
R
Cd36 Expression
S
Wnt6 Expression
Cluster Number
1 2 3 4 5 6 7 8 9 10